Enhanced Performance with Bismuth Ferrite Perovskite in ZnO Nanorod Solid State Solar Cells

Journal:	*Nanoscale*
Manuscript ID:	NR-ART-02-2014-000911.R1
Article Type:	Paper
Date Submitted by the Author:	27-Mar-2014
Complete List of Authors:	Loh, Leonard; Nanyang Polytechnic, School of Engineering; Queen Mary University of London, School of Engineering and Materials Science Briscoe, Joe; Queen Mary, University of London, School of Engineering and Material Science Dunn, Steve; Queen Mary, University of London, School of Engineering and Material Science; Queen Mary University of London, Centre for Materials Research

Nanoscale RSCPublishing

ARTICLE

Enhanced Performance with Bismuth Ferrite Perovskite in ZnO Nanorod Solid State Solar Cells

Cite this: DOI: 10.1039/x0xx00000x

Received 00th January 2012,
Accepted 00th January 2012

DOI: 10.1039/x0xx00000x

www.rsc.org/

Leonard Loh,[a,b] Joe Briscoe*[a] and Steve Dunn[a]

This paper reports for the first time the use of perovskite, bismuth ferrite ($BiFeO_3$ or BFO) on ZnO-based solid state solar cells using only chemical solution methods for materials synthesis. As ZnO has poor chemical stability in acidic and corrosive environments, a buffer method using aminosilane ((3-aminopropyltriethoxysilane or $H_2N(CH_2)_3Si(OC_2H_5)_3$)) coating was used to provide a protective coating on the ZnO nanorods. The aminosilane layer was removed after BFO coating. The solid state solar cells, sensitized by N719, used CuSCN as the hole conductor and tested under 100mW/cm^2, AM 1.5G simulated sunlight. The photovoltaic performance showed current density improvements from 0.64 mA/cm^2 to 1.4 mA/cm^2 and efficiencies from 0.1 % to 0.38 % when comparing between ZnO and ZnO/BFO solar cells. The observed ca 400 % improved performance is shown to result from BFO's role as an electron blocking layer.

Introduction

Recent reports highlighting the increase in performance of perovskite-type materials such as $CH_3NH_3PbI_3$[1–3] and $CsSnI_3$[4] in TiO_2-based photovoltaic devices have led to increasing interest in evaluating these materials in photovoltaic devices. The photovoltaic (PV) effect of ferroelectric materials such as the perovskite $BaTiO_3$,[5] and $LiNbO_3$[6] were studied as early as the 1970s. Since then there have been further studies on other perovskite systems such as KBNNO.[7] In ferroelectric materials, anomalous photovoltages producing greater-than-bandgap voltages[5] have been attributed to the internal polarization of the non-centrosymmetric crystals[6]. One particular material that is multiferroic, coupling both ferroelectric and magnetic properties, is the perovskite structured bismuth ferrite ($BiFeO_3$, or BFO).[8] Despite reports of anomalous photovoltaic properties in BFO-only devices,[9–11] BFO has only been used in solar cell devices in a limited number of reports. These include a bio-templated BFO mesoporous-iodide electrolyte-based DSSC,[12] a CNT/BFO/Pt structure with CdSe quantum dots[13,14] and in an inorganic-organic BFO/P3HT/Au hybrid solid state solar cell.[15]

Stability issues found for photovoltaics that use the liquid electrolytes common for dye-sensitized solar cells has led to the investigation of solid-state alternatives. In these structures the liquid is often replaced with p-type semiconductors such as CuSCN,[16] spiro-OMeTAD,[17,18] and the aforementioned perovskite $CsSnI_3$.[4] Of these, CuSCN is inexpensive, stable in air and easily deposited from solution onto nanostructured substrates.[19]

ZnO was chosen for its higher electron mobility, 205-300 cm^{2}Vs^{-1} and higher electron diffusion coefficient, 1.7×10^{-4} cm^{2}s^{-1}, compared to TiO_2.[20] It is also easily synthesized into 1-D nanorods, which have better electron pathways for carrier collection and can be tailored to increase their surface area by increasing the length and aspect ratio, leading to increased light absorption and greater dye adsorption.

In order to produce a viable photovoltaic, ZnO requires a sensitizer to extend the absorption of light into the visible wavelength. There have been previous reports of ZnO:CuSCN-based photovoltaics using a variety of sensitizers.[21] It has been shown that as-deposited and sintered CdSe gave efficiencies of 0.5 % and 1.5 %[22] under 1 sun illumination. The reported efficiencies when using CdS quantum dots was 0.26 %[23] and 3.2 % for In_2S_3.[24] In systems where an organic dye such as N719 has been used to sensitize the ZnO nanorods, the efficiencies of 1.8 µm length ZnO nanorods was reported to be 0.1 %[25] with this value improving to 1.7 %[26] using 11-12 µm long nanorods.

---

[a] *Centre for Materials Research, School of Engineering and Materials, Queen Mary University of London, United Kingdom. Email: j.briscoe@qmul.ac.uk*
[b] *School of Engineering, Nanyang Polytechnic, Singapore*

As we have described above, there are few reports of BFO being used in photovoltaic devices. In order to determine the impact of BFO on photovoltaic performance we have produced a solid state photovoltaic device using p-type BFO. This was completed using nanorods of n-type ZnO, the dye N719 (*(cis-bis bis(2,2'-bipyridyl-4,4'-dicarboxylato) isothiocyanato ruthenium (II) bis-tetrabutylammonium))* as a sensitizer, copper thiocyanate (CuSCN) to collect holes with Au as the counter electrode. The active materials were deposited using aqueous methods.

As ZnO is chemically unstable in corrosive environments such as acidic[27] or alkaline solutions[28,29] a buffer layer of 3-aminopropyltriethoxysilane ($H_2N(CH_2)_3Si(OC_2H_5)_3$), referred to as aminosilane, was coated onto the ZnO before BFO deposition. This layer was removed during the annealing of the BFO. The standard solid-state dye-sensitized devices with 2.3 µm long ZnO nanorods using N719 sensitizer and CuSCN as the hole conductor give an efficiency of 0.1 %. The addition of BFO to the structure improved the efficiency to 0.38 %, with increases in both photocurrent and open-circuit voltage.

Experimental

Material Synthesis

ZnO nanorods were grown on 2 mm thick, 15 Ω fluorine-doped tin oxide (FTO) coated glass substrates using an aqueous method.[30,31] Seeding was done using 5 mM of absolute ethanolic zinc acetate ($Zn(CH_3CO_2)_2$) by repeated dropping on the conductive face of the substrate, and rinsing with ethanol.[30] This process was repeated for 15 cycles with 3 intermediate anneals at 350 °C for 25 minutes on a hotplate. Seeded substrates were suspended in solutions of 25 mM zinc nitrate ($Zn(NO_3)_2.6H_2O$) and 25 mM of hexamethylenetetramine or HMT ($C_6H_{12}N_4$) in deionised (DI) water at 90 °C for 2.5 hours.[30] This process was repeated a total of 6 times in fresh solutions. The ZnO nanorods were coated with aminosilane by soaking the samples in a solution made up of 4 % 3-aminopropyltriethoxysilane in toluene at 60 °C for 30 minutes before rinsing with toluene. Samples were heated to 90 °C for an hour to remove all solvents. Samples were next spin coated at 5000 rpm with a layer of BFO with 0.075 M, 0.15 M or 0.3 M precursor sol. The sol was prepared from bismuth nitrate pentahydrate ($Bi(NO_3)_3.5H_2O$) and iron nitrate nonahydrate ($Fe(NO_3)_3.9H_2O$) mixed in 2-methoxyethanol ($CH_3OCH_2CH_2OH$), with 20 % by volume of the dehydrating agent, acetic anhydride ($(CH_3CO)_2O$) and 2 % by volume of ethanolamine to adjust the viscosity. Samples were preannealed at 100 °C for 1 minute to stabilize the film followed by 350 °C for 3 minutes on a hot plate. Annealing was then done at 600 °C for 2 hours in air in a furnace. All chemicals used were Sigma Aldrich analytical grade reagents unless otherwise stated.

Solar Cell Device Fabrication

The active layer was first coated with 0.5 mM of a dye sensitizer, N719 from Dyesol for 15 hours, followed by rinsing with absolute ethanol to remove excess dye. Dupont's 25 µm Surlyn film was used as a spacer and as a protective and insulating layer outside the active area. The cells were then spray coated with CuSCN from a prepared solution of 0.2 M CuSCN in dipropyl sulfide[19,32] using an Iwata airbrush system while heating at 90 °C on a hotplate. 150 nm thick Au counter electrodes were sputtered using the Denton Vacuum Explorer 14 thermal evaporator using a power of 125 W, base pressure of 4×10^{-2} mTorr and working pressure of 100 mTorr at ambient temperature in 100 % Argon atmosphere.

Characterisation

All morphology, cross-section and surfaces of the films as well as elemental analysis of the films surface were performed using the Jeol JSM 6701F field emission scanning electron microscope (FESEM). Optical absorbance spectra were measured using the Perkin Elmer Lambda 950 UV visible spectroscopy. To obtain dye loading, the dyes were extracted using 5 ml of 0.1 M NaOH in ethanol/water (volume 1:1) and soaked for 12 hours followed by absorbance measurements in the UV-Vis of the extract. The diffraction peaks of the films were studied using the Panalytical X'pert Pro X-ray diffraction (XRD) with CuK_α 1 radiation at k = 1.54056 Å. Hall measurements at room temperature used a compliance voltage of 5 V, measurement current of 50 µA, magnetic field of 0.5 T for a dwell time of 1 seconds. The photovoltaic were tested with the IVT Solar VS 6820 solar simulator system with a Keithley 2400 source meter to obtain the J-V curve under 100 mW/cm^2, AM 1.5G simulated sunlight. The

Results and Discussion

Fig. 1(a) shows an SEM micrograph of the ZnO nanorods indicating the homogeneous growth of single crystal nanorods in the [0001] direction. To date there have been no reports of depositing a sol of BFO on ZnO due to the low stability of ZnO in high and low pH systems. The BFO in this study was deposited using a sol-gel technique using bismuth nitrate pentahydrate ($Bi(NO_3)_3.5H_2O$) and iron nitrate nonahydrate ($Fe(NO_3)_3.9H_2O$). The resulting sol had a pH of less than 1 reacting with the ZnO immediately (Fig. S1). To prevent dissolution of the ZnO, aminosilane was deposited on the ZnO nanorods.[33] ZnO surface contains chemisorped or physiorbed hydroxyl groups which hydrolyses the aminosilane into silanol (Si-OH). Catalysis of amino groups in the aminosilane occurs only at the ZnO surface, causing condensation into siloxane (Si-O-Si).[34,35] As toluene was used as the solvent, the hydrolysis and condensation occurs only at the surface of the ZnO where the hydroxyl groups exist, and this results in mainly monolayers self-assembled on the surface of ZnO. Annealing the structure at 600 °C after BFO deposition removes the aminosilane to leave BFO-coated ZnO. Three morphologies of BFO – islands, conformal film and thicker conformal film – were deposited on the ZnO nanorods by controlling the concentration of the sol from 0.075 - 0.3 M. Fig. 1 shows BFO-coated ZnO nanorods after annealing at 600°C.

At the lowest concentration, the ZnO nanorods were coated with islands of BFO leading to partial coverage. In our case full coverage was achieved with a sol concentration of 0.15 M

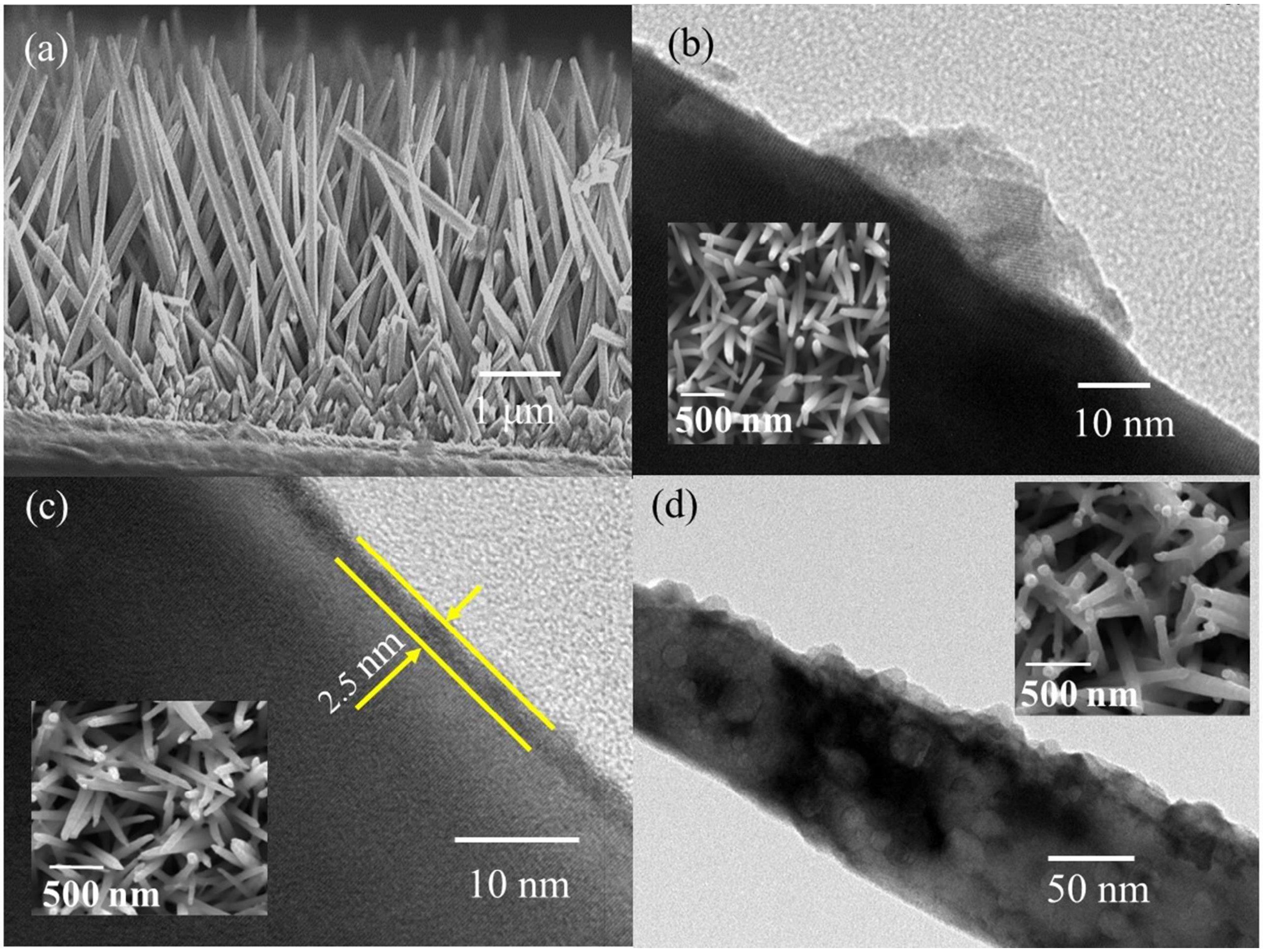

Fig. 1. ZnO nanorods (a) SEM cross section view, (b) Islands of BFO, (c) Conformally coated with BFO, (d) Thicker conformally coated BFO (insets show SEM topographical views)

producing a coating with an average thickness of 2.5 nm. The BFO forms a core-shell structure on the ZnO once a conformal coating has formed. Increasing the molarity of the BFO sol further increases the thickness of the layer. Areas of aggregated BFO give a textured appearance to the coating (Fig. 1).

XRD analysis of the samples post-annealing showed the presence of rhombohedral, R3c BFO crystallinity with the equally strong peaks at the (110) and (104) planes (Fig. 2(a)). The selected area electron diffraction (SAED) pattern of the BFO coated ZnO nanorod sample in Fig. S2 confirms that the surface coating on the ZnO is polycrystalline BFO with (110) and (104) crystal planes. The brighter (104) spot in the SAED data also indicate stronger crystallinity compared to (110), similar to that indicated in the XRD. The HRTEM image also shows strongly crystalline BFO coating. Secondary phases of Bi_2O_3 are seen to appear at higher thickness of BFO. Further

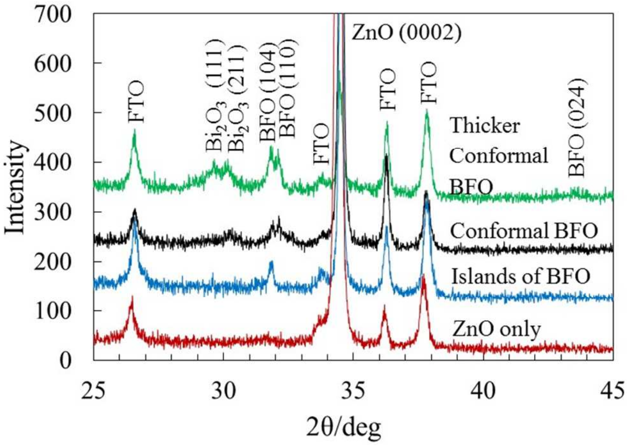

Fig. 2. X-ray diffraction patterns of N719 sensitized ZnO on FTO with varying BFO thicknesses.

examination of the XRD indicates that ZnO has enabled nucleation of the textured BFO during processing due to the close lattice match. N719 sensitization of uncoated or BFO-coated nanorods was achieved by soaking in a dye solution for 15 hours. Good infiltration of the hole conductor, CuSCN, between the ZnO nanorods was achieved by deposition using a spray coating method.[19,32].

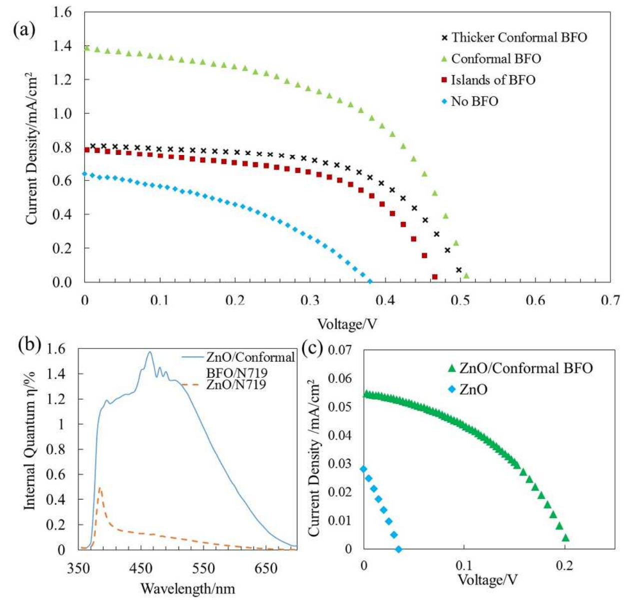

Fig. 3. Current density-voltage curves: (a) comparison of N719 sensitized ZnO solar cells with varying BFO thicknesses under 100 mW/cm^2, 1.5AM illumination, (b) IQE plot of ZnO/N719 and conformal ZnO/BFO/N719 solar cells, (c) comparison of ZnO and conformal ZnO/BFO without N719 solar cells.

Table 1. Performance of N719 sensitized ZnO solid state solar cells with varying BFO thickness

Device Structure	J_{sc} (mA/cm^2)	V_{oc}(V)	FF	η (%)
No BFO	0.64	0.38	0.39	0.10
Islands of BFO	0.79	0.47	0.56	0.20
Conformal BFO	1.4	0.51	0.54	0.38
Thicker Conformal BFO	0.81	0.51	0.57	0.24

Photovoltaic devices were tested under 100 mW/cm^2 AM 1.5G illumination. The J-V characteristics of the photovoltaic devices with different morphologies of BFO and without BFO are shown in Fig. 3(a) and results in Table 1. A ZnO:sensitizer device without BFO (ZnO/N719/CuSCN) produced a J_{sc} of 0.64 mA/cm^2, V_{oc} of 0.38 V with an overall efficiency of 0.1 %, giving equivalent results to that reported previously.[25] For the islands morphology consisting of partial BFO coverage (50-60 % of ZnO exposed), the J_{sc} and V_{oc} increased to 0.79 mA/cm^2 and 0.47 V, and efficiency to 0.2 %. The efficiency increased to 0.38 % with conformally covered BFO at 2.5 nm average thickness, but dropped to 0.24 % with the thicker conformal BFO coating that averaged 7 nm thickness. The V_{oc} increased to 510 mV when the surface of the ZnO was conformally coated, remaining unchanged for the thicker conformal coating. In contrast, J_{sc} increased with BFO coverage up to a maximum of 1.38 mA/cm^2 for the 2.5 nm thick BFO which decreased for the thicker BFO coating. In all cases fill factors (FF) were around 0.55.

The possibility of ferroelectric behaviour in the BFO enhancing the performance was explored. Ferroelectric measurements were conducted on 520 nm thick BFO film deposited on FTO with Au electrodes using a range of charging amplitudes and frequencies. Fig. S4 shows the electric displacement of the BFO film obtained with a charging amplitude of 3.25 V at a frequency of 100 Hz. The voltage and current signals have the same waveforms implying decreasing resistivity with increased voltage. The current density-electric field loops shows contribution from dielectric permittivity as well as electrical conductivity, with the latter being the major contributor. The polarization-electric field loop obtained by integrating the current with respect to time per unit area shows no switching of the domains indicating no ferroelectric hysteresis. Several reports of the difficulty of producing ferroelectric behaviour from BFO film prepared by sol-gel processes[36–38] has been reported, and has been attributed to leakage currents from the fluctuations of the Fe^{3+} and Fe^{2+} as well as the presence of secondary phases.

To explain the improved performance, a variety of other mechanisms were explored that could cause the observed changes to photovoltaic performance upon the addition of the BFO. This includes the photoexcitation of BFO leading to increased light harvesting, interaction with zeta potential of the device surface due to changes in dye loading with the addition of BFO layer, and the role of BFO as an electron blocking layer helping to suppress charge recombination. A discussion of the possible contributions of each of these mechanisms to the enhanced efficiency follows.

Table 2. Performance of ZnO and ZnO/BFO solid state solar cells without N719

Device Structure	J_{sc} (mA/cm^2)	V_{oc}(V)	FF	η (%)
ZnO	0.028	0.04	0.25	0.0003
ZnO/Conformal BFO	0.055	0.21	0.42	0.005

Hall measurements were performed on dense BFO films to determine the majority carrier and semiconductor properties of the material. The measurements confirmed the as deposited BFO to be p-type material[39,40] with hole mobility values of 5–17 cm^{2}V^{-1}S^{-1} and a hole density of 7–27 x 10^{17} cm^{-3}. This means that when combined with ZnO, BFO can form a p-n heterojunction. This will increase electron harvesting through charge separation at the interface, and may influence photovoltaic performance. In order to test this, conformally coated ZnO/BFO/CuSCN photovoltaic structures were fabricated without N719. These structures probed the ability of BFO to photosensitize ZnO in the absence of an organic dye. The J-V curves in Fig. 3(c) and results in Table 2 show that BFO provides only limited photosensitization with very low J_{sc} and V_{oc} values. The equivalent N719 sensitized device in contrast performed 2 orders of magnitude better than the BFO sensitized device. This indicates that the increase in efficiency of N719 sensitized ZnO photovoltaic when BFO was added cannot be attributed to additional photosensitization by the BFO.

Optical absorbance of BFO-coated ZnO in Fig. 4(a), indicates increased absorbance between 380 and 500 nm compared to plain ZnO. This is due to the smaller bandgap of BFO (2.7 eV and increased scattering due to the increased roughness of the BFO-coated surface. The optical absorbance in Fig. 4(b) of N719 sensitized cells show ZnO/N719/CuSCN sample exhibits significantly higher light absorption at wavelengths shorter than 550 nm when compared to the ZnO/BFO/N719/CuSCN samples. In addition, a ZnO/N719/CuSCN device was visually darker than a ZnO/BFO/N719/CuSCN device (Fig. 4c). This gives an indication that there was more dye loading on the ZnO/N719/CuSCN architecture. To quantify differences in dye loading, absorbance of the desorbed dye solution was measured and compared after equivalent soaking times for the two device architectures. A typical ZnO/N719/CuSCN device had 1.01 x 10^{-7} mol cm^{-2} of dye absorbed, compared to 2.92×10^{-8} mol cm^{-2} for a typical ZnO/BFO/N719/CuSCN solar cell. This equates to about a 70 % reduction in dye absorbed on the BFO-coated nanorod and is a significant contribution to the changes in light absorption below 550 nm. It might be expected that the higher dye loading for the BFO-free structures would lead to higher solar cell performance. However, despite the higher dye loading for the ZnO/N719/CuSCN device, its performance was lower than the ZnO/BFO/N719/CuSCN devices.

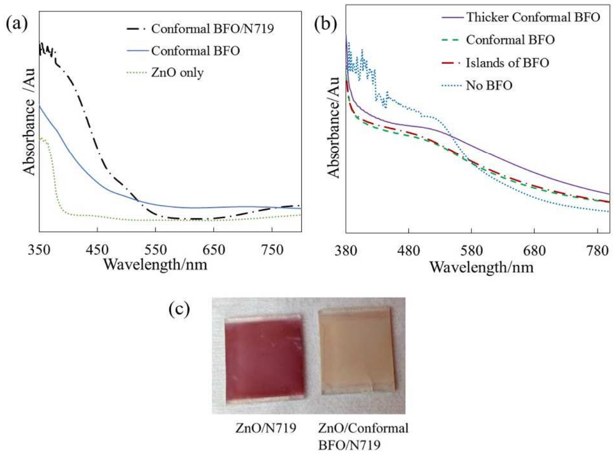

Fig. 4. Comparison of absorbance data for (a) 350 nm ZnO dense film with conformal BFO and N719, (b) N719 sensitized ZnO nanorods with varying BFO thicknesses (c) N719 dye loading

In order to explain this difference we must consider factors beyond light absorption. The occurrence of dye aggregation and formation of Zn^{2+}/dye complexes[41–43] has been reported for N719 dye deposited on ZnO. In these cases dye aggregation caused increased electron recombination within the aggregates, which resulted in decreased electron injection into the ZnO. The optimal pH for N719 sensitization is pH 5. This is below ZnO's point of zero charge (pzc) at pH 9. The positively charged ZnO surfaces attracts protons forming Zn^{2+}/N719 dye complexes which increases dissolution of ZnO[44]. The addition of BFO will reduce dye aggregates as BFO's pzc is pH 6.5[45] closer to the optimal of pH 5 for N719 sensitization. Hence the number of dye aggregates and complexes will be reduced and form a more homogeneous coating of N719.

In addition to the reduction in dye aggregation for BFO-coated systems, the influence of the degree of coverage of BFO on ZnO was considered when assessing the impact on device performance. The indicative energy bands for the ZnO/BFO/N719/CuSCN structure (Fig. 5a) show that the electron affinity of N719 at 3.76 eV[46] is higher than the electron affinity of BFO, commonly considered to be 3.3 eV.[47,48] The energy bands do not allow for simple exciton separation across the N719/BFO interface. However, the J-V curves for the BFO-coated structures (Fig. 3a) clearly show that as the BFO tends towards complete coverage, there is an increase in device performance. As the thickness of the BFO increases the current decreases but V_{oc} remained largely fixed. This implies that there is a thickness dependence on the rate of transfer of electrons from N719 into the ZnO. In order for electron transport to occur, the electrons have to tunnel through the BFO layer from the N719 to reach the ZnO. Considering the BFO layer as a simple square barrier it can be calculated that the probability for electrons to tunnel from N719 to ZnO is negligible above a BFO thickness of around 2 nm (see Fig. S6). The field due to the p-n junction between BFO and ZnO will improve this carrier transfer, therefore increasing slightly the thickness through which carriers will tunnel. This is approximately the thickness of the thinnest conformal BFO coating produced in our work and which achieved the highest efficiency reported here. The principle of tunnelling across the barrier is in agreement with the drop in J_{sc} for the thicker conformal BFO coating, as the majority of this film is greater than 2 nm thick. Thus, although BFO does not act as a solid state sensitizer and directly transfer photogenerated electrons into the ZnO, electrons can tunnel from the N719 to the ZnO through a thin conformal BFO coating but not a thicker coating. This explains the increased photocurrent in the device with the thinner conformal coating compared to the thicker conformal coating, but does not fully explain the optimal performance of the conformal coating compared to the island morphology.

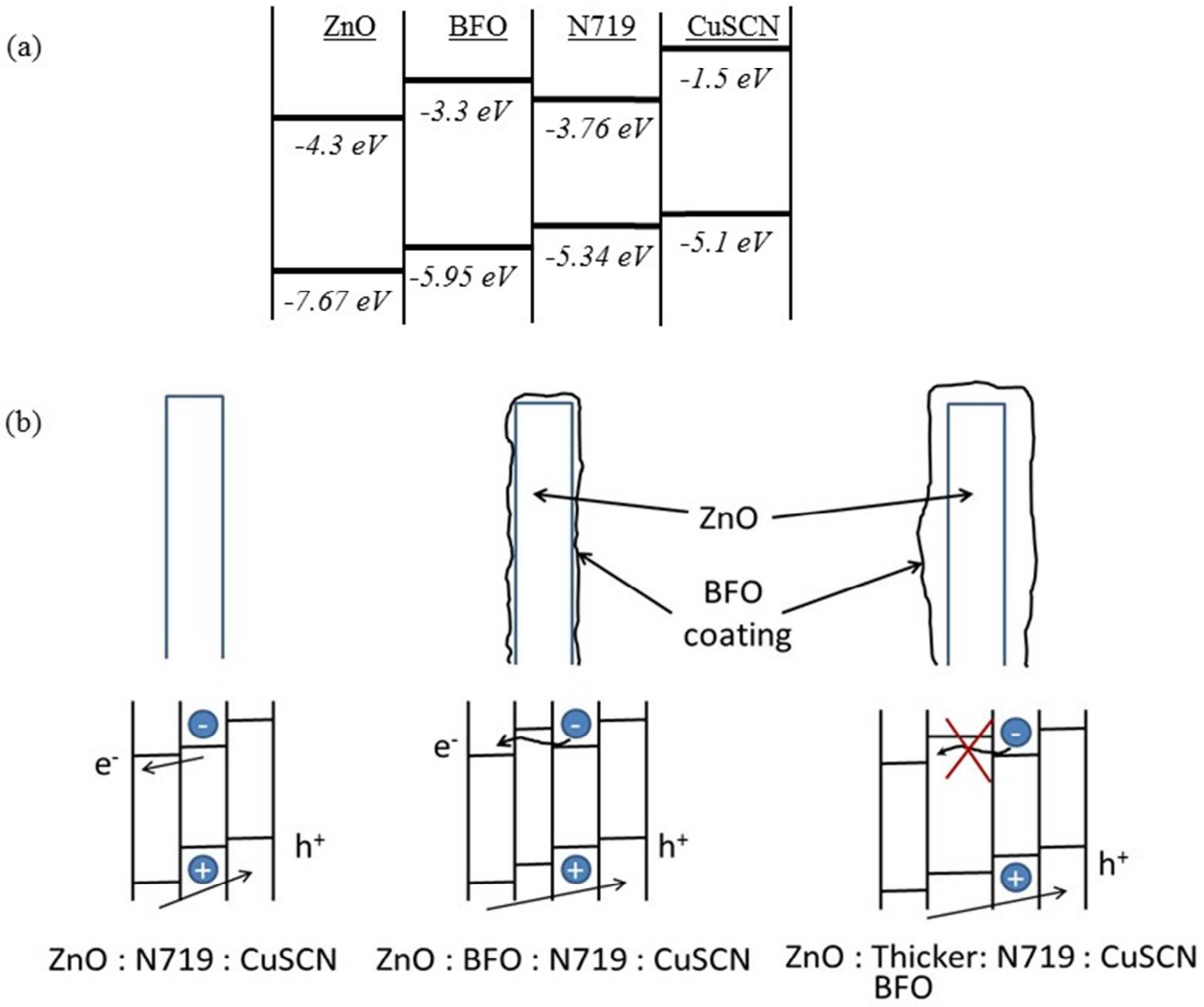

Fig. 5. Schematic representation of (a) Energy bands of ZnO/BFO/N719/CuSCN structure, (b) Charge transport mechanisms of ZnO with varying BFO thicknesses solar cells

A common problem faced by dye sensitized photovoltaic architectures is electron-hole recombination: electrons can recombine with the oxidized dye or as it encounters a hole in the hole conducting layer.[49] The addition of a conformal coating of BFO to ZnO nanorods enables the BFO to act as an electron blocking layer preventing the electron from recombining with oxidized N719. Fig. 5(b) shows a schematic of the carrier transport mechanisms for the three cases of BFO coating, and also plain ZnO with N719. When islands of BFO exist there are regions of ZnO in direct contact with oxidized N719. This structure produces intermediate device efficiency as there are regions where BFO is present which suppresses electron recombination and uncoated regions where the electron recombination rate will be largely unchanged. This decreases overall electron recombination resulting in increased J_{sc}. In the conformally coated sample, electron recombination with the oxidized N719 is blocked. However, electrons are still able to tunnel from the N719 through the BFO into the ZnO which gives the maximum J_{sc}. With thicker conformal coatings, electron recombination is reduced by the same amount as a thinner conformal sample due to the presence of BFO, but electron tunnelling will be reduced due to the increased thickness of the BFO. This will have the net effect of reducing J_{sc}.

The V_{oc} increase for the BFO coated samples can be attributed to a decrease in trap states at the interface[50] and a shift in energy levels at both interfaces due to the addition of the BFO into the structure. Further evidence of a decrease in recombination at the interface can be determined by investigating the source of the decrease in dark current for devices upon addition of BFO (Fig. 6), where different loss mechanisms have been shown to dominate at different applied biases.[51,52] The dark current plots (Fig. 6) show noticeable differences at low and medium applied bias, indicating differences in shunt resistance (dominant < 0.4 V) and series resistance (dominant between 0.4 and 0.7 V), but little difference in space charge limited current mechanisms above 0.7 V.

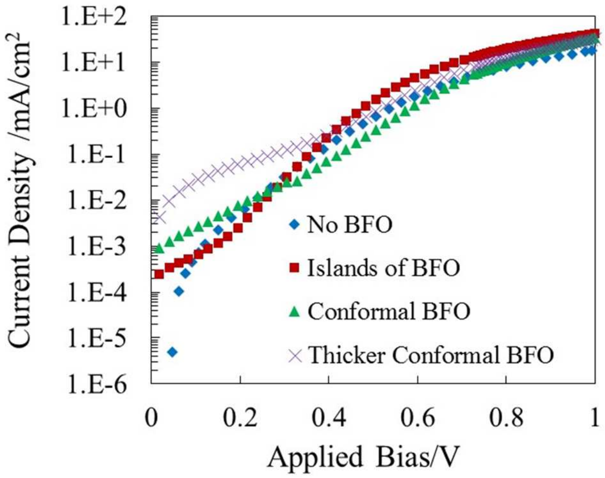

Fig. 6. Dark current-voltage characteristics at room temperature for N719 sensitized ZnO solar cells with varying BFO thicknesses

A sample of plain ZnO/N719/CuSCN demonstrates superior shunt resistance below 0.1 V when compared to all BFO coated samples. However, the improved shunt resistance and ideality factor for the islands BFO morphology sample between 0.1 V and 0.4 V indicate that the addition of BFO improves junction properties. These further improve with the conformal BFO sample, which exhibits improved shunt and series resistance. The changes in ideality factor for the conformal BFO sample was indicative of the electron blocking mechanism associated with the BFO coating. The dark current plot for the thicker conformal BFO sample shows a decrease in ideality factor, indicating a reduction in junction quality. This has previously been attributed to tunnelling mechanism[51] across the barrier. This matches the reduced probability of electron tunnelling through the BFO barrier as described earlier. Hence, we believe that the improvements in V_{oc} with BFO coating stem from an improvement in the diode performance, which drops with the thickest coating due to limitations of tunnelling across the barrier in agreement with the analysis above.

Conclusions

In conclusion, we have presented a method for the production of conformal BFO coating on ZnO nanorods and demonstrated that this system can be used to enhance the performance of a solid state dye-sensitized solar cell. Increases in both J_{sc} and V_{oc} result in an improvement of device efficiency by a factor of 4. It was shown that the BFO does not directly sensitize the ZnO to visible light, but instead limits N719 aggregation due to its zero point potential and acts as an electron blocking layer which prevents electrons from recombining with the N719. These changes to the recombination and interface properties lead to the enhanced performance of the device. We have shown that to achieve this enhancement the thickness of the BFO coating must be carefully controlled, being as thin as possible (< 2 nm) while conformally coating the ZnO. Hence if controlled effectively, this material can be used to enhance the efficiency of solid-state DSSCs, which could lead to increased efficiency with further optimisation of device design.

Acknowledgments

Funding from The Leverhulme Trust is acknowledged.

References

1 L. Etgar, P. Gao, Z. S. Xue, Q. Peng, A. K. Chandiran, B. Liu, M. K. Nazeeruddin, and M. Gratzel, *J. Am. Chem. Soc.*, 2012, **134**, 17396–17399.
2 H.-S. Kim, J.-W. Lee, N. Yantara, P. P. Boix, S. A. Kulkarni, S. Mhaisalkar, M. Gratzel, and N.-G. Park, *Nano Lett.*, 2013, **13**, 2412–2417.
3 A. Kojima, K. Teshima, Y. Shirai, and T. Miyasaka, *J. Am. Chem. Soc.*, 2009, **131**, 6050–6051.
4 I. Chung, B. Lee, J. Q. He, R. P. H. Chang, and M. G. Kanatzidis, *Nature*, 2012, **485**, 486–490.
5 P. S. Brody and F. Crowne, *J. Electron. Mater.*, 1975, **4**, 955–971.
6 A. M. Glass, D. V. D. Linde, and T. J. Negran, *Appl. Phys. Lett.*, 1974, **25**, 233–235.
7 I. Grinberg, D. V. West, M. Torres, G. Gou, D. M. Stein, L. Wu, G. Chen, E. M. Gallo, A. R. Akbashev, P. K. Davies, J. E. Spanier, and A. M. Rappe, *Nature*, 2013, **503**, 509–512.
8 S. R. Basu, L. W. Martin, Y. H. Chu, M. Gajek, R. Ramesh, R. C. Rai, X. Xu, and J. L. Musfeldt, *Appl. Phys. Lett.*, 2008, **92**, 91905.
9 W. Ji, K. Yao, and Y. C. Liang, *Adv. Mater.*, 2010, **22**, 1763–1766.
10 S. Y. Yang, J. Seidel, S. J. Byrnes, P. Shafer, C. H. Yang, M. D. Rossell, P. Yu, Y. H. Chu, J. F. Scott, J. W. Ager, L. W. Martin, and R. Ramesh, *Nat. Nanotechnol.*, 2010, **5**, 143–147.
11. J. Seidel, D. Fu, S.-Y. Yang, E. Alarcón-Lladó, J. Wu, R. Ramesh, and J. W. Ager III, *Phys. Rev. Lett.*, 2011, **107**, 126805.
12. N. Nuraje, X. N. Dang, J. F. Qi, M. A. Allen, Y. Lei, and A. M. Belcher, *Adv. Mater.*, 2012, **24**, 2885–2889.

13. Y. Y. Zang, D. Xie, Y. Chen, X. Wu, T. L. Ren, H. W. Zhu, J. L. Cao, and D. Plant, *J. Appl. Phys.*, 2012, **112**, 054103.
14. Y. Y. Zang, D. Xie, Y. Chen, X. Wu, T. L. Ren, J. Q. Wei, H. W. Zhu, and D. Plant, *Nanoscale*, 2012, **4**, 2926–2930.
15. Z. K. Liu and F. Yan, *Phys. Status Solidi-Rapid Res. Lett.*, 2011, **5**, 367–369.
16. B. O'Regan and D. T. Schwartz, *Chem. Mater.*, 1998, **10**, 1501–1509.
17. U. Bach, D. Lupo, P. Comte, J. E. Moser, F. Weissortel, J. Salbeck, H. Spreitzer, and M. Gratzel, 1998, **395**, 583–585.
18. D. Q. Bi, L. Yang, G. Boschloo, A. Hagfeldt, and E. M. J. Johansson, *J. Phys. Chem. Lett.*, 2013, **4**, 1532–1536.
19. S. M. Hatch, J. Briscoe, and S. Dunn, *Thin Solid Films*, 2013, **531**, 404–407.
20. Q. F. Zhang, C. S. Dandeneau, X. Y. Zhou, and G. Z. Cao, *Adv. Mater.*, 2009, **21**, 4087–4108.
21. J. Briscoe and S. Dunn, *Mater. Sci. Technol.*, 2011, **27**, 1741–1756.
22. R. Tena-Zaera, M. A. Ryan, A. Katty, G. Hodes, S. Bastide, and C. Levy-Clement, *Comptes Rendus Chim.*, 2006, **9**, 717–729.
23. E. Edri, E. Rabinovich, O. Niitsoo, H. Cohen, T. Bendikov, and G. Hodes, *J. Phys. Chem. C*, 2010, **114**, 13092–13097.
24. T. Dittrich, D. Kieven, M. Rusu, A. Belaidi, J. Tornow, K. Schwarzburg, and M. Lux-Steiner, *Appl. Phys. Lett.*, 2008, **93**, 053113.
25. B. Postels, A. Kasprzak, T. Buergel, A. Bakin, E. Schlenker, H. H. Wehmann, and A. Waag, *J. Korean Phys. Soc.*, 2008, **53**, 115–118.
26. U. V Desai, C. K. Xu, J. M. Wu, and D. Gao, *Nanotechnology*, 2012, **23**, 053113.
27. E. Cetinorgu and S. Goldsmith, *J. Phys. D-Applied Phys.*, 2007, **40**, 5220–5226.
28. J. Zhou, N. S. Xu, and Z. L. Wang, *Adv. Mater.*, 2006, **18**, 2432–2435.
29. Y. Yang, D. S. Kim, Y. Qin, A. Berger, R. Scholz, H. Kim, M. Knez, and U. Gosele, *J. Am. Chem. Soc.*, 2009, **131**, 13920–13921.
30. J. Briscoe, D. E. Gallardo, S. Hatch, V. Lesnyak, N. Gaponik, and S. Dunn, *J. Mater. Chem.*, 2011, **21**, 2517–2523.
31. B. Weintraub, Z. Zhou, Y. Li, and Y. Deng, *Nanoscale*, 2010, **2**, 1573–1587.
32. S. M. Hatch, J. Briscoe, and S. Dunn, *Adv. Mater.*, 2013, **25**, 867–871.
33. K. Ogata, H. Dobashi, K. Koike, S. Sasa, M. Inoue, and M. Yano, in *Physica Status Solidi C: Current Topics in Solid State Physics, Vol 7 No 6*, eds. A. Toropov and S. Ivanov, Wiley-V C H Verlag Gmbh, Weinheim, 2010, **7**, 1562–1564.
34. P. Kijkobchai and S. Wacharawichanant, *TIChE Int. Conf. 2011*, 2011, 1–5.
35. F. Grasset, N. Saito, D. Li, D. Park, I. Sakaguchi, N. Ohashi, H. Haneda, T. Roisnel, S. Mornet, and E. Duguet, *J. Alloys Compd.*, 2003, **360**, 298–311.
36. M. M. Kumar, V. R. Palkar, K. Srinivas, and S. V Suryanarayana, *Appl. Phys. Lett.*, 2000, **76**, 2764–2766.
37. Y. Wang, Q. H. Jiang, H. C. He, and C. W. Nan, *Appl. Phys. Lett.*, 2006, **88**, 142503.
38. X. M. Chen, G. D. Hu, X. Wang, J. Yan, C. H. Yang, and W. B. Wu, *J. Mater. Sci.*, 2009, **44**, 3556–3560.
39. Z. Zhang, P. Wu, L. Chen, and J. L. Wang, *Appl. Phys. Lett.*, 2010, **96**, 232906.
40. H. Yang, H. M. Luo, H. Wang, I. O. Usov, N. A. Suvorova, M. Jain, D. M. Feldmann, P. C. Dowden, R. F. DePaula, and Q. X. Jia, *Appl. Phys. Lett.*, 2008, **92**, 102113.
41. K. Keis, C. Bauer, G. Boschloo, A. Hagfeldt, K. Westermark, H. Rensmo, and H. Siegbahn, *J. Photochem. Photobiol. a-Chemistry*, 2002, **148**, 57–64.
42. V. Thavasi, V. Renugopalakrishnan, R. Jose, and S. Ramakrishna, *Mater. Sci. Eng. R-Reports*, 2009, **63**, 81–99.
43. H. J. Snaith and L. Schmidt-Mende, *Adv. Mater.*, 2007, **19**, 3187–3200.
44. T. P. Chou, Q. F. Zhang, and G. Z. Cao, *J. Phys. Chem. C*, 2007, **111**, 18804–18811.
45. S. Li, J. Zhang, M. G. Kibria, Z. Mi, M. Chaker, D. Ma, R. Nechache, and F. Rosei, *Chem. Commun.*, 2013, **49**, 5856–5858.
46. F. De Angelis, S. Fantacci, E. Mosconi, M. K. Nazeeruddin, and M. Graetzel, *J. Phys. Chem. C*, 2011, **115**, 8825–8831.
47. S. J. Clark and J. Robertson, *Appl. Phys. Lett.*, 2007, **90**, 132903.
48. W. Ji, K. Yao, Y.-F. Lim, Y. C. Liang, and A. Suwardi, *Appl. Phys. Lett.*, 2013, **103**, 062901.
49. B. C. O'Regan and F. Lenzmann, *J. Phys. Chem. B*, 2004, **108**, 4342–4350.
50. Y. S. Lee, J. Heo, S. C. Siah, J. P. Mailoa, R. E. Brandt, S. B. Kim, R. G. Gordon, and T. Buonassisi, *Energy Environ. Sci.*, 2013, **6**, 2112–2118.
51. J. Pallares, R. Cabre, L. F. Marsal, and R. E. I. Schropp, *J. Appl. Phys.*, 2006, **100**, 084513.
52. B. Yoo, K. Kim, D.-K. Lee, M. J. Ko, H. Lee, Y. H. Kim, W. M. Kim, and N.-G. Park, *J. Mater. Chem.*, 2010, **20**, 4392–4398.